Nanoscale

ROYAL SOCIETY OF CHEMISTRY

COMMUNICATION

View Article Online
View Journal | View Issue

Cite this: *Nanoscale*, 2025, **17**, 12080

Received 10th December 2024,
Accepted 9th March 2025

DOI: 10.1039/d4nr05209a

rsc.li/nanoscale

Integration of two-dimensional WS_2 in flexible textile triboelectric nanogenerators *via* electronic dyeing for self-powered sensing†

Mashael H. Albuqami,[a,b] Evgeniya Kovalska,[a] Kavya S. Sadanandan,[a] Mashael S. Alghamdi,[a,b] Ana I. S. Neves, [a] Saverio Russo[a] and Monica F. Craciun *[a]

We present flexible textile triboelectric nanogenerators by electronically dyeing polyester with two-dimensional tungsten disulfide (2D WS_2), thereby enhancing its triboelectric properties when paired with nylon. Drop casting, immersion, and spray coating were evaluated, demonstrating their effectiveness in tailoring the fabric's triboelectric properties, showcasing 2D WS_2's potential for self-powered sensors and energy-harvesting applications.

Textile-integrated triboelectric nanogenerators (textile-TENGs)[1–5] have gained attention as promising energy-harvesting and self-powered-sensor systems capable of converting mechanical energy from activities like human motion into usable electricity. Their integration with textiles offers versatility, making them ideal for wearable energy and sensing applications.[6–12] Scalability and compatibility with textile manufacturing pose significant challenges for the large-scale implementation of textile-TENGs. These challenges primarily arise from the use of polymeric triboelectric materials, such as polydimethylsiloxane (PDMS)[13,14] and polytetrafluoroethylene (PTFE),[14,15] which often require fabrication techniques, such as spin coating, dip coating, or layer-by-layer assembly. These methods are less commonly used in textile manufacturing, further complicating their integration into established production processes. To address these limitations, novel approaches are required to tailor the triboelectric properties of textile fabrics for TENG applications.

Among various materials for TENGs, 2D materials[16,17] such as graphene,[18–27] MoS_2,[28–30] $MoSe_2$,[31–33] and WS_2,[34–38] stand out due to their flexibility, stretchability, and washability. 2D WS_2 offers a range of advantages[39–48] such as low cost, low toxicity, and structural tunability, along with high surface charge density and mechanical flexibility, both crucial for efficient energy conversion. As a semiconductor, it exhibits the requisite electronic behaviour for generating and transferring charge in TENGs. Furthermore, with its composition based on tungsten and sulphur rather than other elements found in related materials within the same family,[39] 2D WS_2 offers enhanced stability and performance. Its chemical stability and low friction coefficient are promising for long-term durability and efficient operation during repeated mechanical deformation. These characteristics[40–48] make 2D WS_2 an excellent candidate for enhancing the triboelectric properties of textiles, outperforming other 2D materials in many aspects.

Here, we introduce the concept of using 2D WS_2 as an electronic dye to enhance the performance of textile fabrics in TENGs. By applying a nanoscale 2D WS_2 coating on polyester fabrics, we effectively modify its triboelectric properties, enabling precise control over the fabric's position in the triboelectric series, leveraging 2D WS_2's electronic properties. This method preserves the fabric's inherent flexibility while also providing an eco-friendly and scalable processing solution by using green solvents such as water and isopropanol. To apply 2D WS_2 on the polyester fabric, we employed three textile dyeing methods—drop casting, immersion coating, and ultrasonic spray coating—with spray coating yielding the best performance. These coating techniques offer versatile, scalable methods for incorporating 2D materials into various production stages, from fibres to garments, without compromising the textile characteristics.[19,22,23] We present a flexible single-electrode textile-TENG by integrating 2D WS_2-coated polyester with nylon fabric as the triboelectric pair coupled to a copper electrode. Comprehensive testing of the 2D WS_2-coated polyester was conducted using various counter triboelectric materials [Kapton, nitrile, polyester, *meta*-aramid, paper, rubber, polyethylene terephthalate (PET), polyvinyl chloride (PVC), and nylon] to evaluate device performance on flat textile substrates. We also conducted bending tests with varying radii to evaluate the flexibility of TENGs. Notably, the spray-coated TENGs show minimal performance change after bending, outperforming drop casting and immersion methods

[a]*Centre for Graphene Science, Faculty of Environment, Science and Economy, University of Exeter, UK. E-mail: m.f.craciun@exeter.ac.uk*
[b]*Taif University, Department of Physics, Taif University, Saudi Arabia*
† Electronic supplementary information (ESI) available. See DOI: https://doi.org/10.1039/d4nr05209a

in flexibility. These devices also adapted well to different bending radii. Our study paves the way for cost-effective, self-powered textile sensors and highlights the transformative potential of 2D material-based electronic dyeing in advancing next-generation energy-harvesting and sensing textiles.

The exfoliation of 2D WS_2 was performed using a Silverson L5M high-shear mixer following a procedure similar to that demonstrated for graphene exfoliation.[49] Specifically, 0.25 g of bulk WS_2 powder (Sigma-Aldrich, 2 mm, 99%) was dispersed in a solvent mixture of 75 mL of isopropanol (IPA) and 225 mL of deionized water at a 1 : 3 ratio. The mixture was processed at a rotation speed of 7000 rpm for 2 hours with the high-shear mixer. X-ray diffraction and Raman spectroscopy were employed to confirm the 2D nature of the exfoliated 2D WS_2, with detailed results shown in Fig. S1 in the ESI.†

We employed three methods to deposit 2D WS_2 layers onto polyester textile fabrics (M-09305-A01, 0.32 mm thickness, 269 gsm, Heathcoat Fabrics Ltd): drop casting, immersion, and spray coating. The drop casting method, illustrated in Fig. 1(a), involved applying successive increments of 0.15 mL of 2D WS_2 suspension onto the textile surface, followed by drying inside an oven at 100 °C for 1 h between each layer deposition. To optimize the layer thickness, one (0.15 mL) to twenty (3 mL) successive layers were applied and their performance was evaluated within a TENG device.

Fig. 1 Diagrams of the 3 deposition techniques used: drop casting (a), immersion coating (b), and spray coating (c). Surface morphology and topography of the polyester fabric coated with 2D WS_2 characterised using a 3D light microscope for drop casting (d), immersion coating (e), and spray coating (f) at 200 μm scale. (g)–(r) Corresponding SEM images from 100 μm to 20 μm. (d), (g), (j), (m) and (p) are for the optimal drop casting of 4 layers. The illustrations in (a), (b) and (c) were generated by using Bing AI.

TENG testing demonstrated that a four-layer thickness delivered superior performance compared to other configurations (Fig. S6 in the ESI†). For immersion coating, illustrated in Fig. 1(b), the textile substrate was submerged in a volume of suspension ranging from 0.75 mL to 3 mL placed in a 6 cm diameter glass Petri dish. The setup was heated to 70 °C until the liquid completely evaporated. TENG testing for the immersion method showed that a 0.75 mL suspension provided better performance than the other configurations (Fig. S7 in the ESI†). Spray coating, illustrated in Fig. 1(c), was performed using a Sono-Tek ExactaCoat system with an ultrasonic nozzle (48 kHz) to ensure the uniform dispersion of 2D WS_2. The 2D WS_2 dispersion (1.8 mL and 3 mL) was sprayed at an air pressure of 6.5 bar and a flow rate of 0.7 mL min^{-1} onto the textile substrate placed on a 120 °C hot plate for rapid solvent evaporation. TENG testing for the spray method revealed that a 3 mL suspension resulted in the optimal performance (Fig. S8 in the ESI†).

The surface morphology and topography of the fabric, both before and after 2D WS_2 coating using the three methods, were characterized using a 3D light digital microscope (VHX-7000 series, 4K high-precision) and a scanning electron microscope (TESCAN VEGA3 SEM). Fig. 1(d)–(f) present the 3D microscopy images of textiles coated using drop casting, immersion coating and spray coating techniques, respectively, for a scale of 200 μm.

Fig. 1(g)–(i) show the corresponding SEM images on a 100 μm scale, while Fig. 1(j)–(l) show those on a 50 μm scale and Fig. 1(m)–(o) show those on a 20 μm scale. The images are for the optimal deposition for each method. Additional images, ranging from 1 mm to 10 μm and covering various layer thicknesses as well as the fabric surface before coating, are shown in Fig. S2–S4 in the ESI.† These studies reveal a conformal coating over the texture of textile yarns extending from fabric weaves down to the individual fibre level for all 2D WS_2 coatings applied using the three techniques. For optimal deposition—achieving the highest TENG output when the 2D WS_2-coated polyester is paired with a textile counter-triboelectric layer—the spray coating method provides the most uniform coverage at the fibre level. In comparison, other methods yield only partial fibre coating, with immersion offering slightly better coverage than drop casting. Cross-sectional SEM images for all three deposition methods are shown in Fig. 1(p)–(r), obtained by digital zooming in the low-magnification SEM images at 100 μm. From these images, we estimated the 2D WS_2 coating thickness to be below μm, with comparable average thickness across all deposition methods. However, coating uniformity varies significantly. The ultrasonic spray technique achieved the most consistent coverage, uniformly coating surface fibres, whereas other methods resulted in flake agglomerations primarily on the top of the fibres. We note that

higher magnification imaging for precise thickness measurement was hindered by charging effects due to the non-conductive fabric substrate.

Fig. 2(a) illustrates the flexible textile-TENG used in this study, operating in a single-electrode configuration. As shown in Fig. 2(b), the device (with an area of 1.5 cm × 2.5 cm) integrates a 2D WS_2-coated polyester fabric as one of the triboelectric layers, fabricated using the three methods illustrated in Fig. 1, paired with nylon as the triboelectric counterpart and back-coated with copper as the electrode.

The TENGs were characterised in contact-separation mode using a setup based on Dharmasena *et al.*[50] comprising a horizontal stage with a moving side and a fixed side, as shown in Fig. S5 in the ESI.† The open-circuit voltage (V_{oc}) and short-circuit current (I_{sc}) generated by the TENG devices were recorded using a Keithley 6514 at a contact separation frequency of 1 Hz and are shown in Fig. 2(c–h) for the three deposition methods of 2D WS_2. The TENG's output parameters were monitored during the contact and separation processes of the 2D WS_2-coated polyester and nylon fabrics. This interaction generates positively and negatively charged surfaces due to charge transfer between the two fabrics. In separated mode, a spatial gap between the layers facilitates electron flow from the ground to the nylon coupled to the electrode under the influence of triboelectric potential, while in contact mode, the electrons return to the ground. These results demonstrate that the integration of spray-coated 2D WS_2 into TENGs results in superior voltage and current output (Fig. 2(g) and (h)), outperforming both the drop casting (Fig. 2(c) and (d)) and immersion (Fig. 2(e) and (f)) methods, highlighting the enhanced TENG performance achieved with spray coating.

Nylon was selected as the triboelectric pair for polyester coated with 2D WS_2 due to its textile nature, aligning with the goal of developing textile-TENGs. At the same time, an optimisation study was carried out to investigate various counter triboelectric materials, evaluating their performance when combined with both uncoated polyester and polyester coated with 2D WS_2 layers (prepared by drop casting, immersion, and spray coating) to determine the most effective combination for enhanced TENG performance. This selection process aimed not only to enhance TENG performance but also to ensure that the output voltages are compatible with integration into microcontroller systems for future wireless data collection. By carefully choosing materials with suitable triboelectric properties, we optimised the voltage output, facilitating the potential for self-powered sensing applications in wearable technology and smart textiles. As shown in Fig. 3, each of the uncoated polyester (Fig. 3a) and polyester coated with 2D WS_2 layers prepared by drop casting (Fig. 3b), immersion (Fig. 3c), and spray coating (Fig. 3d) was systematically tested with a range of materials (Kapton, PVC, nitrile, polyester, *meta*-aramid, paper, rubber, PET, and nylon) under consistent conditions to establish the triboelectric series. The triboelectric series established using the short-circuit current data is shown in Fig. S9 in the ESI.† Our data show that the 2D WS_2-coated polyester obtained by immersion/drop-casting paired with paper or PVC generates a higher electrical output than the spray-coated 2D WS_2 polyester paired with nylon due to greater differences in their electron affinity, as indicated by their relative positions in the triboelectric series. Materials with larger electron affinity differences exhibit enhanced charge transfer, leading to increased triboelectric TENG performance. However, since our study focuses on textile-based triboelectric pairs, non-textile

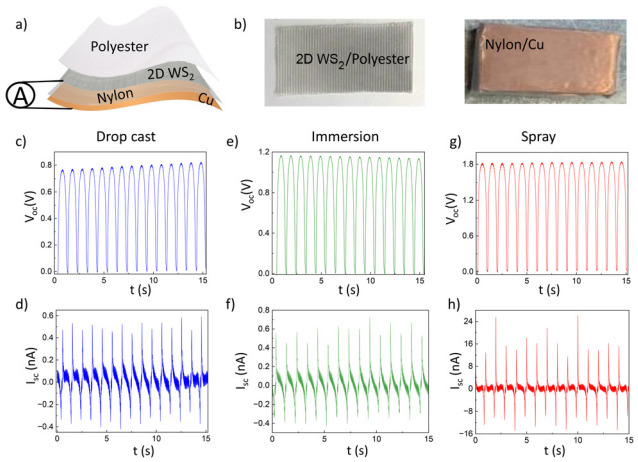

Fig. 2 (a) Schematic of the flexible textile-based triboelectric nanogenerator, working in a single-electrode configuration, fabricated using 2D WS_2 coated onto the polyester fabric as a triboelectric layer, with nylon serving as the counter triboelectric pair and copper acting (Cu) as an electrode. (b) Photographs of the parts of the TENG device with an area of 1.5 cm × 2.5 cm. Open-circuit voltage (V_{oc}) and short-circuit current (I_{sc}) *vs.* time for 2D WS_2 coated *via* drop casting (c) and (d), respectively. V_{oc} and I_{sc} for 2D WS_2 coated *via* immersion (e) and (f), respectively. V_{oc} and I_{sc} for 2D WS_2 coated *via* spray (g) and (h), respectively.

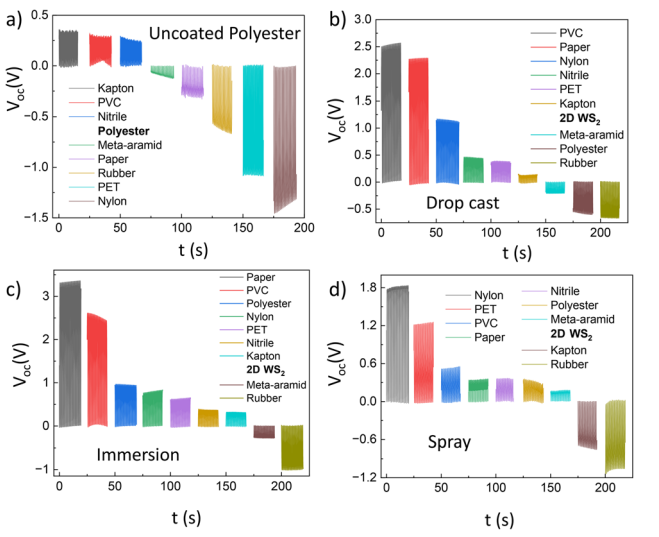

Fig. 3 Triboelectric series based on open-circuit voltage measurements over time for different triboelectric layers of TENGs tested with (a) uncoated polyester, (b) polyester coated with 2D WS_2 *via* drop casting, (c) polyester coated with 2D WS_2 *via* immersion, and (d) polyester coated with 2D WS_2 *via* spray.

materials like paper and PVC were not considered for further applications. Additionally, we observed that while the immersion/drop-cast 2D WS_2 polyester paired with nylon produced a lower electrical output than the spray-coated counterpart, the spray-coated 2D WS_2 polyester with nylon demonstrated improved performance, making it the preferred choice for textile-integrated TENG applications. This configuration produced an open-circuit voltage of approximately 1.8 V.

The position of uncoated polyester in the triboelectric series—between nitrile (less electropositive) and *meta*-aramid (more electropositive)—reflects its balanced triboelectric properties, indicating its relative tendency to donate or accept electrons when in contact with other materials, Fig. 3(a). Specifically, polyester having a moderate electron affinity compared to the other materials is less likely to donate electrons than nitrile but more likely than *meta*-aramid, paper, and rubber. Thus, pairing polyester with materials lower in the series such as nylon maximizes its ability to donate electrons. The data in Fig. 3(b and c) reflect the relative positions of the 2D WS_2-coated polyester in the triboelectric series depending on the coating method, highlighting how the coating technique influences the triboelectric properties.

Polyester coated with 2D WS_2 *via* drop casting appears near the electropositive end (closer to rubber), suggesting a shift toward weaker electron affinity compared to uncoated polyester. The series shows significant rearrangement, with the 2D WS_2-coated polyester positioned closer to the electropositive end, near *meta*-aramid and rubber. Materials such as Kapton and PVC shift towards the middle, reflecting the altered interactions due to the presence of 2D WS_2. The partial coverage of drop casting partially exposes the underlying polyester, contributing to this intermediate position. The coating seems to reduce the electron-donating capacity of polyester, which is consistent with the drop casting method creating only partial 2D WS_2 coverage (Fig. 1g).

For the 2D WS_2-coated polyester obtained *via* immersion, a similar rearrangement occurs, but it shifts slightly further toward the electropositive end compared to the 2D WS_2-coated polyester obtained *via* drop casting. This method positions Kapton, PET, and nylon closer together in the middle of the series. This is consistent with the immersion coating providing more uniform coverage than drop casting (Fig. 1h), enhancing the triboelectric properties but maintaining the trend of 2D WS_2 reducing polyester's electron affinity.

For the 2D WS_2-coated polyester obtained *via* spray coating, the series shows a pronounced shift, and it moves near the electropositive extreme, beyond *meta*-aramid and close to Kapton and rubber. Nylon, PET, and PVC cluster at the opposite end, highlighting a clearer separation of materials with different triboelectric affinities. This is again consistent with spray coating, ensuring the most consistent and complete 2D WS_2 coverage, maximizing its influence on the triboelectric interactions (Fig. 1i).

These results demonstrate that the introduction of 2D WS_2 and the chosen coating method significantly rearrange the triboelectric series. The shifts are not limited to polyester; other materials also adjust their relative positions based on their interactions with the coated surface. Spray coating emerges as the most effective method for enhancing the triboelectric properties, as it produces a uniform 2D WS_2 layer that strongly influences the series, driving the 2D WS_2-coated polyester to the electropositive extreme and redefining the distribution of other materials. This variability highlights the importance of coating techniques in optimising TENG performance.

The data in Fig. 3 also revealed that 2D WS_2 consistently exhibited strong electron-donating properties, making it an effective triboelectric material for self-powered sensing applications when paired with electron-accepting materials like nylon, paper, PET and PVC. On the other hand, 2D WS_2 exhibited electron-accepting properties when paired with electron-donating materials like rubber. On the triboelectric series, 2D WS_2 was positioned between Kapton and *meta*-aramid, indicating its intermediate electron affinity. This suggests that 2D WS_2 can serve as a versatile triboelectric layer, offering tuneable performance when paired with materials of higher or lower positions on the series, thus enhancing the design flexibility of TENG systems.

The TENGs based on 2D WS_2-coated polyester produced *via* the 3 methods were further evaluated for their properties under flat and bent conditions for a fixed bending radius of 5 mm. The results are shown in Fig. 4, showing the performance of the 2D WS_2-coated polyester obtained *via* immersion and drop-casting paired with PVC, as well as the 2D WS_2 spray-

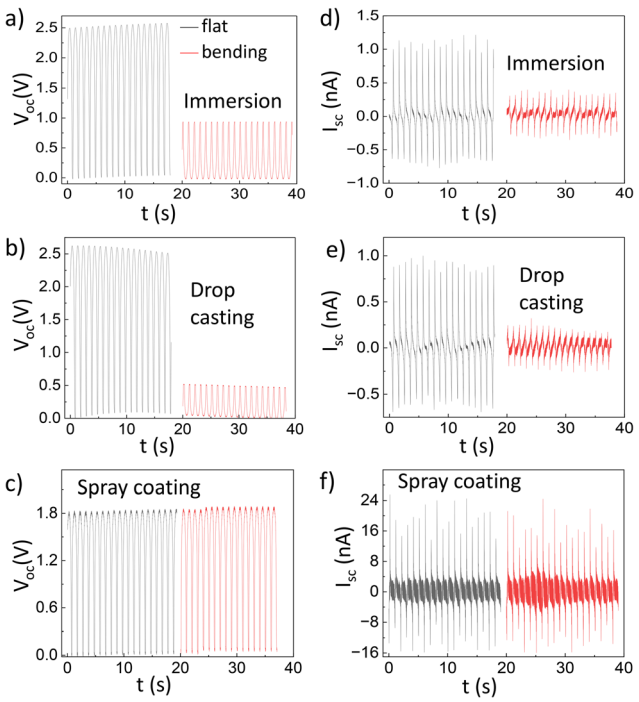

Fig. 4 Open-circuit voltage and short-circuit current of TENG devices in the flat position and after bending 5 mm with the 2D WS_2 device prepared by immersion (a and d), drop casting (b and e), and spray coating (c and f). The counter triboelectric layer is PVC for drop casting and immersion and nylon for spray coating.

coated polyester paired with nylon, the optimal triboelectric pairing. The measurements for the 2D WS_2 spray-coated polyester paired with PVC under flat and bent conditions are shown in Fig. S10 in the ESI.†

The results revealed limited flexibility and stability for immersion and drop casting with a significant reduction in performance, as the output response drop ped by half under bending compared to their flat configuration. In contrast, the TENGs based on the 2D WS_2-coated polyester produced *via* spray coating demonstrated superior flexibility and stability. Only minor variations in the output voltage and short-circuit current were observed between the flat and bent states, demonstrating the robustness of spray coating.

To further investigate 2D WS_2's flexibility and its capacity to withstand textile distortion, bending tests with various bending radii were conducted. Cylinders corresponding to various bending radii were utilised as supports (Fig. 5a and b) for each sample, ranging from no bending to 50 mm, with measurements taken before and after bending. Fig. 5 shows the performance dependence on the bending radius for the 2D WS_2-coated polyester obtained *via* immersion and drop-casting paired with PVC, as well as for the 2D WS_2 spray-coated polyester paired with nylon. For comparison, the performance of the 2D WS_2 spray-coated polyester paired with PVC under both flat and bent conditions is presented in Fig. S11 in the ESI.† Notably the device prepared by the spray coating method exhibited an unchanged behaviour in both the output voltage and short-circuit current. In contrast, significant alterations in behaviour were observed in the drop casting and immersion coating methods.

The bending test results overall highlight the advantages of the spray coating method for 2D WS_2-coated textiles, particularly in terms of flexibility and mechanical stability. While devices prepared *via* immersion and drop casting experienced a reduction in performance under bending, they still demonstrated functional capabilities. In contrast, TENGs based on the 2D WS_2-coated polyester produced *via* spray coating showed superior performance with only minor variations in the output voltage and short-circuit current between the flat and bent states. These findings demonstrate the robustness of the spray coating method, making it particularly suitable for applications requiring frequent mechanical deformation, such as wearable and flexible devices, while immersion and drop casting remain viable options for less mechanically demanding applications.

The enhanced flexibility of the spray-coated samples can be attributed to the uniformity of the coating, as confirmed by SEM analysis and supported by the water contact angle and surface energy measurements shown in Fig. 6. Water adhesion energy (W_a) and surface free energy (γ_p) were calculated using Young–Dupré equations: $W_a = \gamma_w(1 + \cos\theta)$ and $\gamma_p = \gamma_w/4(1 + \cos\theta)^2$, where θ is the contact angle at equilibrium and γ_w is the water surface energy (73 mJ m^{-2}). The SEM images in Fig. 1 show that the spray deposition method results in a more continuous and conformal coating that evenly covers the fibre surfaces, whereas drop casting and immersion lead to some agglomerations and uneven coverage of the fibre surface. The more uniform distribution in the spray-coated samples minimises localized stress points that could otherwise cause cracking and delamination during mechanical deformation, enhancing the mechanical stability of the coating. Furthermore, the significantly higher water contact angle of 135° for the spray-coated samples corresponds to a much lower surface free energy (1.6 mJ m^{-2}) and water adhesion energy (21.4 mJ m^{-2}), indicating a more complete and hydrophobic coverage of the 2D WS_2 material. In contrast, drop-casting (20°) and immersion (35°) exhibit much higher surface free energies (68.7 mJ m^{-2} and 60.4 mJ m^{-2}, respectively) and correspondingly higher adhesion energies (141.6 mJ m^{-2} and 132.8 mJ m^{-2}), suggesting stronger interactions with water and a less uniform coating. The uncoated polyester surface (25° contact angle) also shows a relatively high surface free energy (66.3 mJ m^{-2}) and adhesion energy (139.2 mJ m^{-2}), further emphasizing the distinct hydrophobic nature of the spray-coated layer. A lower surface free energy reduces interfacial stress accumulation and improves the coating's ability to deform without cracking, as it decreases strong intermolecular interactions that could lead to mechanical failure under strain. Additionally, the hydrophobic

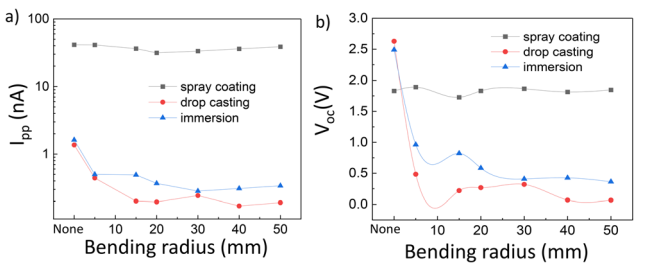

Fig. 5 Summary of measurements after bending tests with varying bending radii, ranging from no bending to 50 mm, for the samples produced by the three different deposition methods. Panel (a) shows the peak-to-peak short-circuit current (I_{pp}) and panel (b) shows the open-circuit voltage. The counter triboelectric layer is PVC for drop casting and immersion and nylon for spray coating.

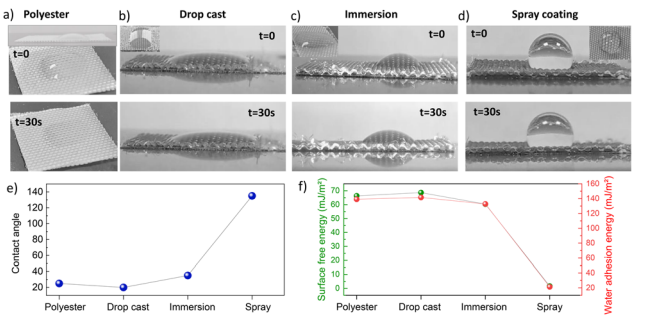

Fig. 6 Photographs of the water contact angle for polyester (a) and polyester coated with 2D WS_2 by drop casting (b), immersion (c), and spray coating (d). The wettability measurement was carried out using a goniometer and the contact angle (e) was analysed using an online screen protractor. (f) Surface free energies and water adhesion energies for the different samples.

nature of the spray-coated layer prevents moisture absorption, which could otherwise alter the coating's mechanical properties and lead to premature degradation. Furthermore, the water absorption behaviour of uncoated polyester, where the droplet is fully absorbed within 30 seconds (Fig. 6a), contrasts sharply with the 2D WS_2-coated polyester, where the droplet remains stable on the surface for all coating methods (Fig. 6b–d). This indicates a significant shift from a hydrophilic to a hydrophobic surface, as confirmed by the lower surface free energy of the coated samples. This combination of a uniform morphology, a lower surface free energy, and a reduced adhesion energy contributes to greater mechanical flexibility, allowing the spray-coated samples to withstand repeated bending without significant loss of performance, ensuring durability.

Conclusions

This study focuses on leveraging 2D WS_2 as a triboelectric layer in textile TENGs, aiming to combine eco-friendly materials with scalable manufacturing approaches for advancing wearable self-powered sensing solutions. In this work, we introduce the concept of electronic dyeing, referring to the process of applying materials with desirable electronic properties—such as 2D WS_2—onto textile fabrics to enhance their functional characteristics. Inspired by conventional textile dyeing processes, electronic dyeing modifies surface properties such as triboelectric performance rather than colour. We explored various deposition methods, including ultrasonic spray coating, drop casting, and immersion techniques, to integrate liquid-phase-exfoliated 2D WS_2 into textile fabrics. These methods allow for the seamless incorporation of 2D WS_2 while maintaining the flexibility and wearability of textiles, enhancing their triboelectric properties. Among the approaches, spray coating demonstrated superior uniformity and mechanical stability, making it particularly effective for flexible applications. Our investigation highlights cost-effective and straightforward approaches for manufacturing 2D WS_2 on fabrics while emphasizing the exceptional suitability of 2D WS_2 as a triboelectric layer. The results demonstrate the significant potential of 2D WS_2-based TENGs for use in flexible and wearable technologies, providing a robust foundation for advancing self-powered sensing and energy-harvesting applications using 2D WS_2 nanostructures.

Data availability

The data supporting this article have been included as part of the ESI.†

Conflicts of interest

There are no conflicts to declare.

Acknowledgements

The authors would like to acknowledge the funding provided by the Engineering and Physical Sciences Research Council (EPSRC), UK, *via* awards EP/S019855/1, EP/M001024/1, EP/V052306/1, and EP/M002438/1 and the EPSRC Centre for Doctoral Training in Meta-materials at the University of Exeter (EP/L015331/1). M. H. Albuqami and M. S. Alghamdi acknowledge financial support from the Saudi Arabia Cultural Bureau. For the purpose of open access, the author has applied a 'Creative Commons Attribution (CC BY) licence to any Author Accepted Manuscript version arising from this submission.

References

1 W. Seung, M. K. Gupta, K. Y. Lee, K. S. Shin, J. H. Lee, T. Y. Kim, S. Kim, J. Lin, J. H. Kim and S. W. Kim, *ACS Nano*, 2015, **9**, 3501.
2 J. Q. Xiong, P. Cui, X. L. Chen, J. X. Wang, K. Parida, M. F. Lin and P. S. Lee, *Nat. Commun.*, 2018, **9**, 4280.
3 Z. M. Lin, J. Yang, X. S. Li, Y. F. Wu, W. Wei, J. Liu, J. Chen and J. Yang, *Adv. Funct. Mater.*, 2018, **28**, 1704112.
4 X. Pu, L. X. Li, H. Q. Song, C. H. Du, Z. F. Zhao, C. Y. Jiang, G. Z. Cao, W. G. Hu and Z. L. Wang, *Adv. Mater.*, 2015, **27**, 2472–2478.
5 Z. Z. Zhao and Y. F. Hu, *Adv. Mater. Technol.*, 2024, **9**, 21.
6 V. U. Somkuwar, A. Pragya and B. Kumar, *J. Mater. Sci.*, 2020, **55**, 5177.
7 J. Song, B. Yang, W. Zeng, Z. H. Peng, S. P. Lin, J. Li and X. M. Tao, *Adv. Mater. Technol.*, 2018, **3**, 1800016.
8 E. Kovalska, H. T. Lam, Z. Saadi, R. Mastria, A. I. S. Neves, S. Russo and M. F. Craciun, *Nano Energy*, 2024, **120**, 109109.
9 Y. Y. Mao, Y. Li, J. Y. Xie, H. Liu, C. J. Guo and W. B. A. Hu, *Nano Energy*, 2021, **84**, 105918.
10 L. Y. Ma, R. H. Wu, A. Patil, J. Yi, D. Liu, X. W. Fan, F. F. Sheng, Y. F. Zhang, S. Liu, S. Shen, J. Wang and Z. L. Wang, *Adv. Funct. Mater.*, 2021, **31**, 2102963.
11 S. Wang, S. Liu, J. Y. Zhou, F. X. Li, J. Li, X. F. Cao, Z. Y. Li, J. S. Zhang, B. S. Li, Y. Wang and X. L. Gong, *Nano Energy*, 2020, **78**, 105291.
12 J. Q. Xiong, P. Cui, X. L. Chen, J. X. Wang, K. Parida, M. F. Lin and P. S. Lee, *Nat. Commun.*, 2018, **9**, 4280.
13 J. Huang, S. Wang, X. Zhao, W. Zhang, Z. Chen, R. Liu, P. Li, H. Li and C. Gui, *Mater. Horiz.*, 2023, **10**, 3840.
14 K. Dong, Y. Hu, J. Yang, *et al.*, *MRS Bull.*, 2021, **46**, 512.
15 Y. Miao, M. Zhou, J. Yi, *et al.*, *Nano Res.*, 2024, **17**, 5540.
16 S. J. Kim, K. Choi, B. Lee, Y. Kim and B. H. Hong, *Annu. Rev. Mater. Res.*, 2015, **45**, 63.
17 I. Ali, N. Karim and S. Afroj, *EcoMat*, 2024, **6**, e12471.
18 D. W. Shin, M. D. Barnes, K. Walsh, D. Dimov, P. Tian, A. I. S. Neves, C. D. Wright, S. M. Yu, J. B. Yoo, S. Russo and M. F. Craciun, *Adv. Mater.*, 2018, **30**, 1802953.

19 I. Domingos, Z. Saadi, K. S. Sadanandan, H. A. Pocinho, D. M. Caetano, A. I. S. Neves, M. F. Craciun and H. Alves, *Nano Energy*, 2023, **115**, 108688.
20 I. Domingos, A. I. S. Neves, M. F. Craciun and H. Alves, *Front. Phys.*, 2021, **9**, 742563.
21 D. Nutting, J. F. Felix, E. Tillotson, D. W. Shin, A. De Sanctis, H. Chang, N. Cole, S. Russo, A. Woodgate, I. Leontis, H. A. Fernández, S. J. Haigh and F. Withers, *Nat. Commun.*, 2020, **11**, 3047.
22 K. S. Sadanandan, Z. Saadi, C. Murphy, I. Grikalaite, M. F. Craciun and A. I. S. Neves, *Nano Energy*, 2023, **116**, 108797.
23 K. S. Sadanandan, A. Bacon, D.-W. Shin, S. F. Alkhalifa, S. Russo, M. F. Craciun and A. I. Neves, *J. Phys.: Mater.*, 2020, **4**, 014004.
24 S. Kim, M. K. Gupta, K. Y. Lee, A. Sohn, T. Y. Kim, K. S. Shin, D. Kim, S. K. Kim, K. H. Lee, H. J. Shin, D. W. Kim and S. W. Kim, *Adv. Mater.*, 2014, **26**, 3918.
25 Z. G. Yan, L. L. Wang, Y. F. Xia, R. D. Qiu, W. Q. Liu, M. Wu, Y. Zhu, S. L. Zhu, C. Y. Jia, M. M. Zhu, R. R. Cao, Z. L. Li and X. Wang, *Adv. Funct. Mater.*, 2021, **31**, 2100709.
26 L. Shi, H. Jin, S. R. Dong, S. Y. Huang, H. Z. Kuang, H. S. Xu, J. K. Chen, W. P. Xuan, S. M. Zhang, S. J. Li, X. Z. Wang and J. K. Luo, *Nano Energy*, 2021, **80**, 105599.
27 Y. Chen, B. Xie, J. Y. Long, Y. C. Kuang, X. Chen, M. X. Hou, J. Gao, S. Zhou, B. Fan, Y. B. He, Y. T. Zhang, C. P. Wong, Z. A. K. Wang and N. Zhao, *Adv. Mater.*, 2021, **33**, 2104290.
28 H. Q. Gao, M. A. Hu, J. F. Ding, B. L. Xia, G. L. Yuan, H. S. Sun, Q. H. Xu, S. Y. Zhao, Y. W. Jiang, H. Wu, M. Yuan, J. H. Li, B. X. Li, J. Zhao, D. W. Rao and Y. N. Xie, *Adv. Funct. Mater.*, 2023, **33**, 2213410.
29 H. Zhang, D. Z. Zhang, R. Y. Mao, L. N. Zhou, C. Q. Yang, Y. Wu, Y. K. Liu and Y. C. Ji, *Nano Energy*, 2024, **127**, 109753.
30 P. Gajula, J. U. Yoon, I. Woo, S. J. Oh and J. W. Bae, *Nano Energy*, 2024, **121**, 109278.
31 Y. Zheng, X. Li, M. L. Zheng, G. Cheng, Y. L. Zi, S. B. Cheng, H. Z. Cui and X. Y. Li, *Adv. Funct. Mater.*, 2024, **34**, 2307669.
32 V. Singh, S. Rana, R. Bokolia, A. K. Panwar, R. Meena and B. Singh, *J. Alloys Compd.*, 2024, **978**, 173416.
33 W. W. Wang, D. Y. Wang, X. X. Zhang, C. Q. Yang and D. Z. Zhang, *Nanomaterials*, 2022, **12**, 4274.
34 T. Chekke, R. Narzary, S. Ngadong, B. Satpati, S. Bayan and U. Das, *J. Electron. Mater.*, 2024, **53**, 238.
35 T. Chekke, R. Narzary, S. Ngadong, B. Satpati, S. Bayan and U. Das, *J. Electron. Mater.*, 2023, **52**, 2685.
36 Y. H. Sun, W. Z. Song, D. J. Sun, T. Zhang, D. S. Zhang, J. Zhang, S. Ramakrishna and Y. Z. Long, *Appl. Phys. Lett.*, 2023, **123**, 153901.
37 T. Chekke, R. Narzary, S. Ngadong, B. Satpati, S. Bayan and U. Das, *Sens. Actuators, A*, 2023, **349**, 114076.
38 M. Baraily, B. Baro, R. Boruah and S. Bayan, *Nanotechnology*, 2024, **35**, 365502.
39 M. Chhowalla, H. Shin, G. Eda, *et al.*, *Nat. Chem.*, 2013, **5**, 263.
40 Y. Chen and M. Sun, *Nanoscale*, 2021, **13**, 5594.
41 D. Liang, C. Zhang, C. Shen, *et al.*, *Tribol. Lett.*, 2025, **73**, 12.
42 C. X. Li, D. D. Sang, S. H. Ge, L. R. Zou and Q. L. Wang, *Molecules*, 2024, **29**, 3341.
43 Y. C. Chen and M. T. Sun, *Nanoscale*, 2021, **13**, 5594.
44 A. Afroozeh, E. Akbari and P. Yupapin, *J. Nanoelectron. Optoelectron.*, 2019, **14**, 1225.
45 H. X. Yu, M. Y. Zhang, Y. T. Cai, Y. L. Zhuang and L. L. Wang, *Catalysts*, 2023, **13**, 1148.
46 M. G. Bianchi, F. Risplendi, M. R. Fiorentin and G. Cicero, *Adv. Sci.*, 2024, **11**, 2305162.
47 M. Pumera and A. H. Loo, *TrAC, Trends Anal. Chem.*, 2014, **61**, 49.
48 H. Wang, C. C. Huang and T. Polcar, *Sci. Rep.*, 2019, **9**, 12570.
49 K. L. Ng, B. M. Maciejewska, L. Qin, C. Johnston, J. Barrio, M.-M. Titirici, I. Tzanakis, D. G. Eskin, K. Porfyrakis, J. Mi and N. Grobert, *ACS Sustainable Chem. Eng.*, 2023, **11**, 58.
50 R. D. G. I. Dharmasena, K. D. G. I. Jayawardena, C. A. Mills, R. A. Dorey and S. R. P. Silva, *Nano Energy*, 2018, **48**, 391.